Ventromedial hypothalamic nucleus neuronal subset regulates blood glucose independently of insulin

Jonathan N. Flak,[1] Paulette B. Goforth,[2] James Dell'Orco,[1] Paul V. Sabatini,[1] Chien Li,[3] Nadejda Bozadjieva,[4] Matthew Sorensen,[5] Alec Valenta,[5] Alan Rupp,[1] Alison H. Affinati,[1] Corentin Cras-Méneur,[1] Ahsan Ansari,[1] Jamie Sacksner,[1] Nandan Kodur,[1] Darleen A. Sandoval,[4] Robert T. Kennedy,[5] David P. Olson,[6] and Martin G. Myers Jr.[1]

[1]Department of Internal Medicine and [2]Department of Pharmacology, University of Michigan, Ann Arbor, Michigan, USA. [3]Novo Nordisk, Seattle, Washington, USA. [4]Department of Surgery, [5]Department of Chemistry, and [6]Division of Endocrinology, Department of Pediatrics, University of Michigan, Ann Arbor, Michigan, USA.

To identify neurons that specifically increase blood glucose from among the diversely functioning cell types in the ventromedial hypothalamic nucleus (VMN), we studied the cholecystokinin receptor B–expressing (CCKBR-expressing) VMN targets of glucose-elevating parabrachial nucleus neurons. Activation of these VMN^{CCKBR} neurons increased blood glucose. Furthermore, although silencing the broader VMN decreased energy expenditure and promoted weight gain without altering blood glucose levels, silencing VMN^{CCKBR} neurons decreased hlepatic glucose production, insulin-independently decreasing blood glucose without altering energy balance. Silencing VMN^{CCKBR} neurons also impaired the counterregulatory response to insulin-induced hypoglycemia and glucoprivation and replicated hypoglycemia-associated autonomic failure. Hence, VMN^{CCKBR} cells represent a specialized subset of VMN cells that function to elevate glucose. These cells not only mediate the allostatic response to hypoglycemia but also modulate the homeostatic setpoint for blood glucose in an insulin-independent manner, consistent with a role for the brain in the insulin-independent control of glucose homeostasis.

Introduction

The brain plays crucial roles in the control of most mammalian homeostatic systems, from hormone secretion to fluid and electrolyte balance. The pioneering findings of Claude Bernard in 1849 also suggest roles for the brain in the control of blood glucose (1), as do recent studies demonstrating that the activation of brain regions such as the ventromedial hypothalamic nucleus (VMN) can increase blood glucose levels (2, 3). Because the brain has not been shown to dissociate the defended level of blood glucose from control by the islet, however, the role for the brain in glucose homeostasis has generally been thought of as subservient to peripheral regulators of blood glucose (e.g., insulin and glucagon secretion by pancreatic islets and the sensitivity of the liver and muscle to these hormones) (3, 4).

In contrast, it is well accepted that the brain contains systems that increase hepatic glucose production (HGP) by promoting the secretion of catecholamines, glucagon, glucocorticoids, and some pituitary hormones (e.g., adrenocorticotrophic hormone and growth hormone) during the counterregulatory response (CRR) to hypoglycemia (5). This allostatic system plays a crucial role in the defense against hypoglycemia during insulin treatment in individuals with diabetes, but attenuates after repeated exposure to severe hypoglycemia, a condition known as hypoglycemia-associated autonomic failure (HAAF), thus predisposing individuals to more frequent and severe episodes of hypoglycemia (6).

Although other brain systems probably also contribute to HGP, a variety of data suggest a crucial role for the VMN in the CRR (4, 7–9). Indeed, optogenetic activation of the VMN (using *Sf1^{Cre}*, which broadly targets all VMN neural populations) mimics the CRR (2), as does activation of VMN glucokinase (Gck) neurons (3). The VMN contains many neurons with diverse actions, however, including not only neurons that increase blood glucose and contribute to the CRR but also neurons that promote energy expenditure (10). Indeed, interfering with glutamatergic transmission throughout the VMN decreases energy expenditure and interferes with glucose tolerance as well as blunts the CRR (7), and most manipulations that interfere with overall VMN function primarily decrease energy expenditure, promoting obesity and glucose intolerance (7, 11–16). Indeed, to the extent that roles in glucose homeostasis for specific VMN subpopulations have been investigated, most of these roles were found to involve modulation of energy expenditure and glucose disposal. For instance, infusion of leptin or melanocortin agonists into the VMN does not elevate blood glucose levels but rather promotes glucose uptake and utilization (2, 17–19).

The lack of a molecular marker specific for the subpopulation of VMN neurons that elevates blood glucose has hampered our understanding of the roles played by these cells in physiology and pathophysiology and the mechanisms by which they mediate their effects. To identify VMN neurons that participate in the CRR, we took advantage of our previous finding that cholecystokinin-containing (CCK-containing) neurons in the parabrachial nucleus (PBN) modulate the amplitude of the CRR in response to nutritional signals (20, 21). These PBN^{CCK} neurons project to the VMN, and CCK neurotransmission is required for their stimulation of glucose production (as well as for the endogenous CRR), indicat-

Conflict of interest: CL is an employee of Novo Nordisk. DPO and MGM receive research funding from Novo Nodisk.

Submitted: October 8, 2019; **Accepted:** February 20, 2020; **Published:** May 4, 2020.
Reference information: *J Clin Invest*. 2020;130(6):2943–2952.
https://doi.org/10.1172/JCI134135.

ing the importance of CCK-responsive VMN neurons in the CRR (21). In contrast to peripheral CCK, which modulates appetite via the cholecystokinin A receptor (CCKAR) (22), the VMN contains a large population of cholecystokinin B–expressing (CCKBR-expressing) neurons. Here we reveal the specificity of these VMN^{CCKBR} neurons for increasing blood glucose and demonstrate their roles in the insulin-independent homeostatic control of blood glucose as well as in the CRR.

Results

Because CCK neurotransmission plays a crucial role in the CRR and in the ability of VMN-projecting PBN CCK neurons to elevate blood glucose (20, 21), we generated a *Cckbr*^{Cre}-knockin mouse line to test the potential specificity of VMN^{CCKBR} cells for increasing blood glucose. Crossing *Cckbr*^{Cre} with the Cre-inducible *Rosa26*$^{EGFP\text{-}L10a}$ reporter line revealed the expected distribution of reporter expression across many brain areas in these $Cckbr^{EGFP\text{-}L10a}$ mice, including a substantial population of VMN^{CCKBR} cells (Figure 1A and Supplemental Figure 1; supplemental material available online with this article; https://doi.org/10.1172/JCI134135DS1), the main population of hypothalamic *Cckbr*-expressing cells. As expected, Cre reporter expression in the *Cckbr*^{Cre} mice colocalized with *Cckbr* mRNA by ISH (Supplemental Figure 1). Cre-dependent rabies virus–mediated single-synapse retrograde tracing (23, 24) revealed the expected strong innervation of VMN^{CCKBR} cells by PBN neurons (among other afferents) (Supplemental Figure 2). Importantly, VMN^{CCKBR} neurons represent a subpopulation of VMN neurons that is distinct from VMN^{LepRb} cells (which do not increase blood glucose, ref. 2), although translating ribosome affinity purification of EGFP-expressing ribosomes from $Cckbr^{EGFP\text{-}L10a}$ mice revealed the expression of a variety of other VMN markers in VMN^{CCKBR} cells (Supplemental Figure 3).

To determine the function of VMN^{CCKBR} cells, we injected AAV-DIO-ChR2-eYFP (25) into the VMN of *Cckbr*^{Cre} or *Sf1*^{Cre} mice to express channelrhodopsin (ChR2) specifically in VMN^{CCKBR} cells ($CCKBR^{ChR2}$ mice) or across all populations of VMN neurons ($SF1^{ChR2}$ mice), respectively (Figure 1B and Supplemental Figure 4). The VMN-specific delivery of Cre-inducible adeno-associated virus (AAV) vectors ensures expression specifically in VMN^{CCKBR} cells. Delivering blue light via an optical fiber implanted immediately dorsal to the VMN thus permitted the optogenetic activation of these VMN neuronal populations. We found that activation of VMN^{CCKBR} cells increased blood glucose levels even more effectively than did activation of all VMN cell populations in $SF1^{ChR2}$ mice (Figure 1, C and D). Optogenetic activation of VMN^{CCKBR} cells increased plasma epinephrine, norepinephrine, and corticosterone, consistent with their activation of the sympathetic nervous system (SNS) and adrenal components of the CRR (Figure 1, E–G). In contrast, optical stimulation of VMN^{CCKBR} neurons failed to alter glucagon or insulin concentrations in $CCKBR^{ChR2}$ mice (Figure 1, H–J), suggesting that VMN^{CCKBR} cells can modulate blood glucose independently of changes in islet hormone concentrations. Given the amount of blood required and the small size of the mice, we did not measure pituitary hormone levels during this experiment.

To define the physiologic functions of VMN^{CCKBR} cells relative to the broader VMN, we injected AAV-DIO-TetTox-EGFP (26) into the VMN of *Cckbr*^{Cre} or *Sf1*^{Cre} mice to express tetanus toxin (TT) in these sets of neurons, thus silencing them by preventing their neurotransmitter release (Figure 2 and Supplemental Figure 5). We found that broadly silencing the VMN ($SF1^{TT}$ mice) decreased energy expenditure (VO_2) and increased body weight (BW) and measures of adiposity without altering food intake, whereas silencing VMN^{CCKBR} neurons ($CCKBR^{TT}$ mice) did not perturb any of these parameters (Figure 2, B–F). Thus, although some VMN cells control energy expenditure, these energy expenditure–controlling VMN neurons must be distinct from VMN^{CCKBR} cells.

Although $SF1^{TT}$ mice displayed unchanged glucose but increased circulating insulin concentrations (commensurate with the insulin resistance that accompanies obesity), $CCKBR^{TT}$ mice had decreased blood glucose concentrations compared with controls in both the ad libitum–fed and fasted states (Figure 3, A and B), revealing a physiological role for VMN^{CCKBR} neurons in determining blood glucose concentrations. In contrast, the obesity and insulin resistance of $SF1^{TT}$ mice presumably countermanded the effect of silencing VMN^{CCKBR} neurons in these animals, preventing any decrease in blood glucose. Glucagon was increased and insulin tended to be lower in $CCKBR^{TT}$ mice compared with control mice (Figure 3, B and C), indicating a directionally appropriate response of circulating islet hormone concentrations to low glucose concentrations. Furthermore, pancreatic β cell mass tended to be lower in $CCKBR^{TT}$ mice (Figure 3D), consistent with a chronically lower demand for insulin production in these animals. We observed no detectable change in activity or circulating corticosterone levels in either model (Supplemental Figure 6). These findings suggest that islet-independent processes underlie at least part of the hypoglycemia seen in $CCKBR^{TT}$ mice.

To directly test the notion that VMN^{CCKBR} neurons play a β cell–independent role in the control of glucose homeostasis, we treated $CCKBR^{TT}$ and control mice with streptozotocin (STZ), which ablates β cells and causes insulinopenic diabetes (ref. 27 and Figure 4). As expected, STZ-treated control mice became hyperglycemic (blood glucose >400 mg/dL) and lost approximately 20% of their BW over the 2 weeks of the experiment. In contrast, silencing VMN^{CCKBR} neurons mitigated the hyperglycemia and weight loss associated with STZ diabetes, despite similarly low insulin levels and β cell mass (and similarly elevated corticosterone) in STZ-treated control and $CCKBR^{TT}$ mice, and despite increased glucagon in $CCKBR^{TT}$ mice compared with controls. Thus, VMN^{CCKBR} neurons can modulate the blood glucose setpoint independently of β cell integrity and islet hormone concentrations.

To understand how VMN^{CCKBR} cells might mediate glycemic control, we initially examined glucose clearance in an i.p. glucose tolerance test (GTT) performed in $CCKBR^{TT}$ mice (Figure 5A). Because initial blood glucose concentrations differed between $CCKBR^{TT}$ and control mice (Figure 3A), we compared the change in blood glucose concentrations (rather than absolute glucose concentrations) in this assay. We found that glucose tolerance was not different between $CCKBR^{TT}$ and control mice, suggesting that the relative hypoglycemia of the $CCKBR^{TT}$ mice was unlikely to result from increased glucose clearance. Indeed, glucose infusion to normalize blood glucose in $CCKBR^{TT}$ mice during a basal glucose clamp normalized endogenous insulin levels and revealed decreased glucose clearance as well as decreased HGP in these mice (Figure 5, B–F). These data suggest that suppression of HGP

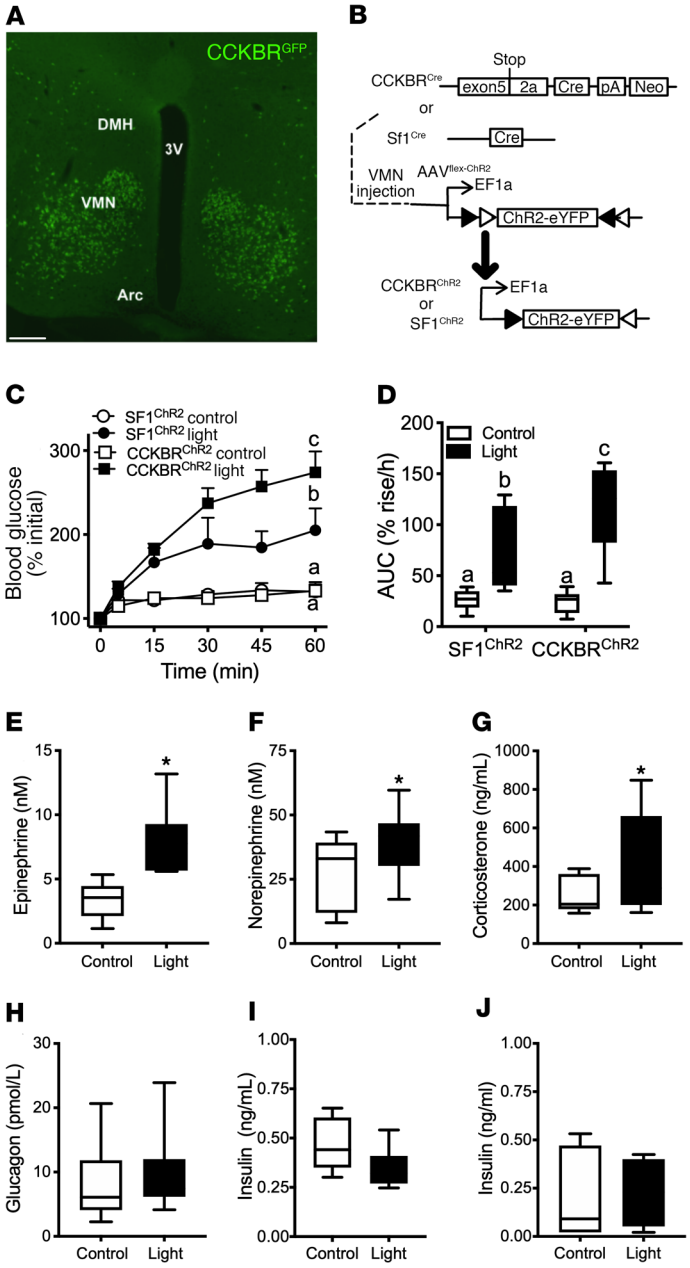

Figure 1. Activation of VMN^{CCKBR} neurons promotes hyperglycemia. (**A**) Shown is a representative image of the VMN from *Cckbr^{Cre}* animals on the *Rosa26$^{EGFP-L10a}$* reporter line stained for GFP (green). 3V, third cerebral ventricle; DMH, dorsomedial hypothalamic nucleus; Arc, arcuate nucleus. Scale bar: 100 μm. (**B**) Experimental schematic showing intra-VMN administration of AAV-DIO-ChR2-eYFP to *Cckbr^{Cre}* (n = 9) or *Sf1^{Cre}* (n = 5) mice to permit the optogenetic activation of VMN^{CCKBR} neurons or all VMN cell populations, respectively. (**C** and **D**) Animals were food deprived at the onset of the light cycle and studied 4–5 hours later. Shown is the glycemic response to control or light delivery, along with the calculated AUC. Plasma samples taken after 30 minutes (**E**, **F**, and **I**) or 60 minutes (**G**, **H**, and **J**) of stimulation in CCKBR^{ChR2} mice were analyzed for circulating concentrations of epinephrine (**E**), norepinephrine (**F**), corticosterone (**G**), glucagon (**H**), and insulin (**I** and **J**). Data are plotted as the mean ± SEM (**C**) or as box-and-whisker plots that show the data spread from minimum to maximum, median, first quartile, and third quartile (**D**–**J**). $P < 0.05$, by 2-way ANOVA with Fisher's LSD post hoc test (**C** and **D**) (the different lowercase letters in the plots in **C** and **D** indicate statistical differences); *$P < 0.05$, by unpaired Student's t test (**E**–**I**).

underlies the low blood glucose levels in CCKBR^{TT} mice. The normalization of insulin levels in CCKBR^{TT} mice upon normalization of blood glucose is consistent with the unaltered responsiveness of the β cell to glucose concentrations in these mice. Overall, these data reveal that VMN^{CCKBR} neuron activity is required for normal homeostatic control of blood glucose by promoting HGP independently of changes in islet hormones.

To understand the potential roles for VMN^{CCKBR} neurons in the CRR, we also examined the response of CCKBR^{TT} mice to insulin-induced hypoglycemia (IIH) (Figure 6A). CCKBR^{TT} mice showed more dramatic hypoglycemia during IIH than did controls, consistent with our prediction that VMN^{CCKBR} neurons play a crucial role in the CRR to hypoglycemia and that interfering with VMN^{CCKBR} neurons should blunt the CRR. To test this directly, we treated CCKBR^{TT} mice with 2-deoxyglucose (2-DG), a glycolytic inhibitor that mimics decreased cellular glucose, thereby activating the CRR independently of insulin to increase HGP (Figure 6B). Indeed, CCKBR^{TT} mice had blunted 2-DG–stimulated glycemic excursion, confirming the role for VMN^{CCKBR} cells in mediating the CRR.

To understand potential roles for VMN^{CCKBR} neurons in HAAF, we subjected control and CCKBR^{TT} mice to a HAAF induction protocol by repeated glucoprivation with 2-DG (Figure 6C). As expected, repeated glucoprivation induced a HAAF-like state in control animals, dramatically blunting the 2-DG–stimulated glucose excursion on day 4 relative to day 1. Interestingly, the impaired day 4 response of control mice was similar to the day 1 response of CCKBR^{TT} mice, and 4 days of 2-DG–mediated glucoprivation failed to alter the glycemic response to 2-DG in CCKBR^{TT} mice. Thus, silencing VMN^{CCKBR} cells mimicked HAAF, and repeated glucoprivation failed to further decrease the CRR in CCKBR^{TT} mice, consistent with the notion that a defect in VMN^{CCKBR} cells contributes to HAAF induction.

To determine whether repeated glucoprivation also impairs the ability of VMN^{CCKBR} neurons to increase blood glucose, we examined the effect of repeated glucoprivation on the ability of optogenetic stimulation of VMN^{CCKBR} neurons to increase blood glucose (Figure 6D). Indeed, we found that repeated glucoprivation blunted the hyperglycemic response to light stimulation in CCKBR^{ChR2} mice. Thus, repeated glucoprivation prevented VMN^{CCKBR} neurons from increasing blood glucose, suggesting that a HAAF-associated lesion lies in the VMN^{CCKBR} neurons or in the downstream circuits that they control.

Discussion

Although the VMN is known to play a role in the CRR, this nucleus contains many distinct neural populations with different functions, including the promotion of glucose utilization and energy expenditure (2, 10). We studied the VMN^{CCKBR} subpopulation to determine the potential specificity of these cells for increasing blood glucose and found that they did not participate in the control of energy expenditure, but rather elevated the blood glucose setpoint during normal physiology as well as increased blood glucose during the CRR (Supplemental Figure 8). Furthermore, VMN^{CCKBR} neurons modulated blood glucose by controlling HGP independently of islet hormones, demon-

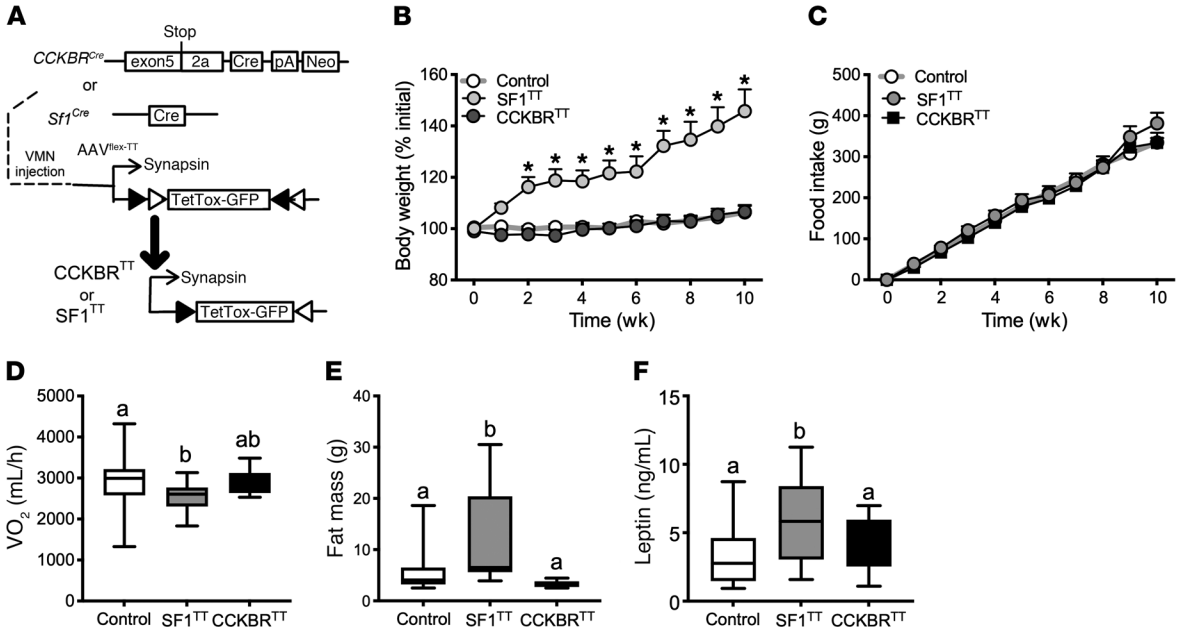

Figure 2. Silencing VMN^{SF1} neurons, but not VMN^{CCKBR} neurons, decreases energy expenditure and causes obesity. (**A**) We injected AAV-DIO-TetTox-EGFP bilaterally into the VMN of *Cckbr*^{Cre} (n = 15) or *Sf1*^{Cre} (n = 11) mice and examined the effects on parameters of energy and glucose homeostasis. Control mice (n = 30) received AAV-GFP; data from control mice of both genotypes are shown merged. Shown are (**B**) BW, (**C**) food intake, (**D**) VO_2, (**E**) fat mass, and (**F**) serum leptin levels. Data are expressed as the mean ± SEM (**B** and **C**) or as box-and-whisker plots showing the data spread from minimum to maximum, median, first quartile, and third quartile (**D**–**F**). *P < 0.05, by 1-way ANOVA (**D**–**F**) or 2-way repeated-measures ANOVA (**B** and **C**) with Fisher's LSD post hoc test (**B**). The different lowercase letters in the plots in **D**–**F** indicate significant differences (P < 0.05).

strating a role for the brain in the control of glucose homeostasis in a manner not subservient to peripheral signals.

Several lines of evidence support the ability of the brain to control blood glucose levels (4). Not only can CNS maneuvers alter energy expenditure and glucose uptake to modulate glucose tolerance (14, 15, 28, 29), but activation of the CRR by the injection of glucoprivic agents into the CNS (8, 9, 30) and global stimulation of the VMN (2, 31) increase blood glucose. Thus, CNS systems control glucose utilization and glucose output. Furthermore, the finding that interfering with glutamatergic neurotransmission by the VMN or inhibiting VMN *Gck* neurons not only impairs glucose utilization and the CRR but also decreases fasted blood glucose suggested that the VMN plays homeostatic roles in supporting blood glucose levels as well as controlling glucose disposal (3, 7).

Our findings reveal not only that VMN^{CCKBR} neurons specialize in increasing blood glucose levels but also that they mediate this effect independently of islet hormones. The insulin independence of the effects of VMN^{CCKBR} contrasts with the control of insulin secretion by glucose-modulating VMN *Gck* neurons; VMN *Gck* neurons also modulate food intake, unlike VMN^{CCKBR} cells (3). The observation that the optogenetic activation of VMN^{CCKBR} cells increases blood glucose more dramatically than the activation of VMN^{SF1} neurons may reflect the countermanding activity of non-*Cckrb* VMN cells that increase glucose uptake and utilization during activation of VMN^{SF1} cells. Indeed, although we and Meek et al. (2)found that optogenetic stimulation of VMN^{SF1} neurons increased blood glucose levels, the activation of Gq-coupled receptors in VMN^{SF1} neurons increased glucose disposal (32), suggesting that the activation of Gq-coupled receptors may preferentially promote the activity of the non-VMN^{CCKBR} cells.

Silencing VMN^{CCKBR} cells decreased blood glucose despite low insulin and high glucagon levels in normal animals and in insulinopenic STZ-treated mice, demonstrating both the ability of these neurons to modulate blood glucose without altering islet hormones and that VMN^{CCKBR} neurons altered blood glucose despite what should be countermanding input from the islet. Similarly, activating VMN^{CCKBR} cells increased blood glucose without elevating glucagon or suppressing insulin. It is worth noting, however, that insulin levels did not increase in response to the hyperglycemia caused by activating VMN^{CCKBR} neurons, which it would be expected to do as a consequence of glucose-stimulated insulin release. Thus, although VMN^{CCKBR} neurons could clearly alter blood glucose without altering islet function, it is possible that these cells might also play some role in suppressing insulin secretion.

Although VMN^{CCKBR} cells did not control blood glucose via the modulation of islet hormones, we found that their activation increased circulating catecholamines and corticosterone, suggesting that their main actions may be mediated via the SNS and adrenal function. Presumably, tissues involved in glucose and energy liberation (e.g., liver and white adipose tissue) represent the main targets for VMN^{CCKBR} cell–mediated SNS activation. Given the low glucose output by mice with silenced VMN^{CCKBR} cells despite their elevated glucagon levels, VMN^{CCKBR} cell–mediated SNS output to the liver and/or liberation of metabolic fuels from adipose or other tissues may be required for effective glucose production. Because there was no change in corticosterone in the CCKBR^{TT} mice, the control of SNS function may be more important than glucocorticoids for the effects of CCKBR^{VMN} cells. In contrast, other VMN cells, such as leptin-

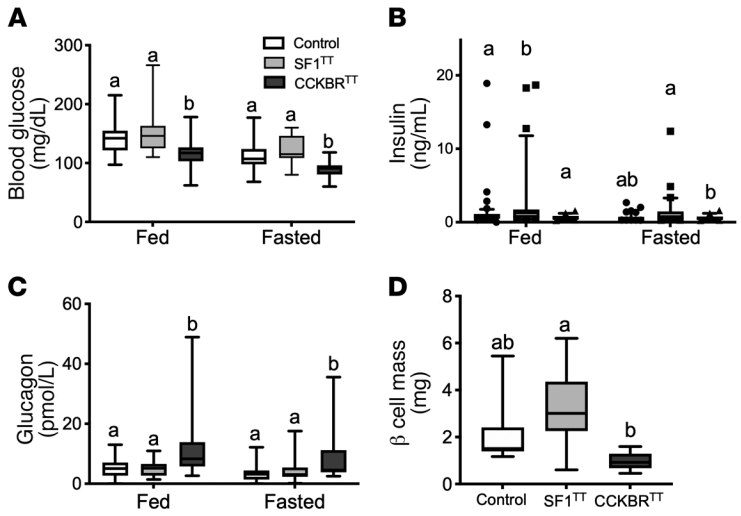

Figure 3. Silencing VMN^{CCKBR} cells causes hypoglycemia. Parameters of glucose homeostasis in SF1^{TT} and CCKBR^{TT} mice were examined. Shown are blood glucose (**A**), serum insulin (**B**), and glucagon (**C**) under ad libitum–fed (10 am) and 24-hour–fasted (10 am to 10 am) conditions. (**D**) Pancreatic β cell mass. Data are expressed as the mean ± SEM or as box-and-whisker plots showing the data spread from minimum to maximum, median, first quartile, and third quartile. n = 54 (control); n = 31 (SF1^{TT}); n = 27 (Cckbr^{TT}). Data were analyzed by 1-way ANOVA with Fisher's LSD post hoc test. The different lowercase letters in the plots indicate significant differences ($P < 0.05$).

responsive cells, appear to mediate their promotion of glucose uptake and energy expenditure via SNS outflow to brown adipose tissue and skeletal muscle (17, 18).

In addition to their roles in glucose homeostasis, VMN^{CCKBR} cells mediated the CRR to insulin-induced hypoglycemia and glucoprivation. Furthermore, the silencing of VMN^{CCKBR} neurons mimicked the HAAF-like response to repeated glucoprivation, and repeated glucoprivation abrogated the ability of VMN^{CCKBR} neuron stimulation to increase blood glucose levels. Thus, VMN^{CCKBR} neurons lie within the neural circuit affected by experimental HAAF. Further work will be required to determine whether HAAF-induced increases in VMN GABA action (33) affect these cells.

In addition to being potentially affected by HAAF, inappropriate activation of VMN^{CCKBR} cells could promote dysglycemia in type 2 diabetes. Thus, VMN^{CCKBR} cells represent potential targets for therapeutic intervention in several diabetes-related pathologic conditions. In the future, it will be important to determine whether HAAF-associated lesions lie in VMN^{CCKBR} neurons themselves, or rather in downstream circuits controlled by VMN^{CCKBR} neurons, and to identify potential roles for VMN^{CCKBR} neurons in type 2 diabetes.

Methods

Animals. All mice were provided food and water ad libitum, unless otherwise noted, and were kept in a temperature-controlled room on a 12-hour light/12-hour dark cycle. *Sf1^{Cre}* mice were previously described (17). To generate *Cckbr^{Cre}* mice, a selection cassette containing the porcine teschoviral 2A cleavage sequence linked to Cre recombinase and a FRT-flanked neomycin resistance gene was targeted to replace the stop codon of the *Cckbr* gene in a bacterial artificial chromosome (Children's Hospital Oakland Research Institute, Oakland, California, USA). A targeting plasmid containing the Cre coding sequences plus the selection cassette and approximately 4 kb genomic sequence upstream and downstream of the *Cckbr* stop codon was isolated and used for embryonic stem cell targeting by the University of Michigan Transgenic Core. Correctly targeted clones were identified by loss of native allele quantitative PCR from ES clone DNA. Chimeric animals generated from blastocyst implantation were then bred for germline transmission of the *Cckbr^{Cre}* allele. Mice expressing Flp recombinase in the germline were then used to remove the neomycin selection cassette. Genotyping was done by allele-specific PCR.

Some *Cckbr^{Cre}* mice were bred onto the *Rosa26$^{EGFP-L10a}$* background (34) to generate Cckbr$^{EGFP-L10a}$ mice in order to visualize Cre-expressing cells and permit translating ribosome affinity purification–sequencing (TRAP-Seq) analysis of VMN^{CCKBR} cells. All experiments were performed using approximately equal numbers of male and female mice. Animals were processed and studied in the order of their randomly assigned ear tag number. Investigators were blinded to the genotype and/or treatment for all studies. All mice were genotyped via PCR across the genomic region of interest before experiments. All mice were bred within our colony.

TRAP-Seq analysis. Adult male and female Cckbr$^{EGFP-L10a}$ mice were anesthetized and their brains removed to a mouse coronal brain matrix (1-mm sections) to isolate the VMN; material from 4 to 6 animals was pooled to produce each sample. mRNA was isolated from EGFP-tagged ribosomes as well as from the EGFP-depleted fraction, as previously described (35). RNA was assessed for quality using the TapeStation System (Agilent Technologies). Samples with RNA integrity numbers (RINs) of 8 or greater were prepped using the Illumina TruSeq LT mRNA Sample Prep Kit (Illumina), and 0.1–3 μg total RNA was converted to mRNA using polyA purification. The mRNA was fragmented via chemical fragmentation and copied into first-strand cDNA using reverse transcriptase and random primers. The 3′ ends of the cDNA were adenylated and 6-nucleotide barcoded adapters ligated. The products were purified and enriched by PCR to create the final cDNA library. Final libraries were checked for quality and quantity using the TapeStation System (Agilent Technologies) and qPCR using the KAPA Library Quantification Kit for Illumina Sequencing platforms (Kapa Biosystems, catalog KK4835). The libraries were clustered on the cBot (Illumina) and sequenced as a 50-cycle, single-end run on a HiSeq 2000 (Illumina) using LT reagents according to the manufacturer's protocols. Single-end reads of 50 bp underwent quality control analysis using FastQC, version 0.11.7 (https://www.bioinformatics.babraham.ac.uk/projects/fastqc/), and filtering of low-quality reads (below Phred 20) was performed using the fastq_quality_filter from the FASTX ToolKit, version 0.0.14 (http://hannonlab.cshl.edu/fastx_toolkit/), before alignment to the mouse genome GRCm38 (mm10, Ensembl, version 92)

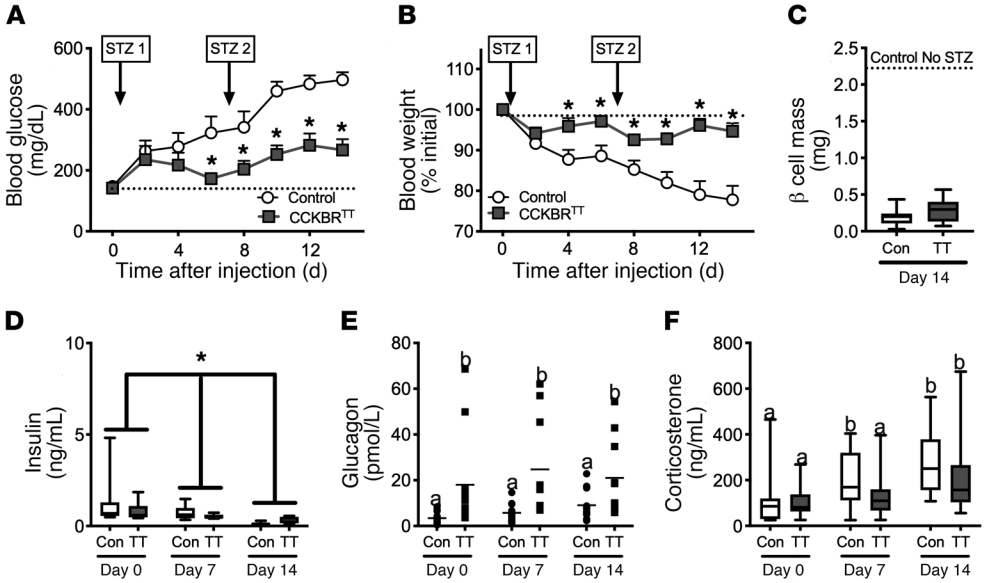

Figure 4. Silencing VMN^{CCKBR} neurons ameliorates insulin-deficient diabetes. AAV-DIO-TetTox-EGFP (CCKBR^{TT}) or AAV-GFP (control) was injected bilaterally into the VMN of *Cckbr^{Cre}* mice. Four weeks later, β cells were ablated in control (n = 14) and Cckbr^{TT} (n = 12) mice by weekly i.p. administration of STZ, and (**A**) glucose, (**B**) BW, and (**D**–**F**) circulating hormone concentrations were assessed. (**C**) β Cell mass was determined at the end of the experiment. Data are expressed as the mean ± SEM (**A** and **B**) or as box-and-whisker plots showing the data spread from minimum to maximum, median, first quartile, and third quartile (**C**–**F**). *P < 0.05 versus control, by 2-way repeated-measures ANOVA with Fisher's LSD post hoc test (**A**, **B**, and **D**–**F**) or Students t test (**C**). The different lowercase letters in the plots in **E** and **F** indicate significant differences (P < 0.05). Con, control.

with STAR 2.5.3_modified (https://github.com/alexdobin/STAR). Enrichment for specific transcripts was determined by comparing gene counts between immunoprecipitated and supernatant material using DESeq2, version 1.22.2 (Bioconductor, https://bioconductor.org/packages/release/bioc/html/DESeq2.html).

Reagents. AAV-TVA+G helper viruses were used as previously described (24); virus stocks were prepared at the University of North Carolina (UNC) Vector Core (Chapel Hill, North Carolina, USA). In addition, the UNC Vector Core prepared AAV-DIO-TT. The rabies-ΔG-mCherry was used as previously described (24) and was generated at the University of Michigan Viral Vector Core with the support of the Molecular Genetics Core of the Michigan Diabetes Research Center (University of Michigan, Ann Arbor, Michigan, USA). AAV-DIO-ChR2-eYFP and AAV-GFP were purchased from the UNC Vector Core.

Stereotaxic injections of viral constructs. Eight- to 14-week-old animals were anesthetized with 1.5% to 2% isoflurane in preparation for craniotomy. After exposing the skull, bregma and lambda were leveled, a hole was drilled, and the contents of a pulled pipette at the coordinates of our target for approximately 25 nL/min were released. For the VMN, 100 nL virus was injected at anteroposterior (AP) –1.2, mediolateral (ML) ±0.3, and dorsoventral (DV) –5.55. For the bed nucleus of the stria terminalis (BST), 100 nL virus was injected at AP 1.1, ML 0.75, and DV –4. All AAVs were packaged by the UNC Vector Core. After 5 minutes, to allow the virus to diffuse into the brain, the pipette was raised slowly from the hole in the skull, the hole in the skull was filled with bone wax, and the skin was closed with surgical sutures (Henry Schein). Analgesics were administered prophylactically to all mice to prevent postsurgical pain. Except for food intake studies, the animals were allowed 4 weeks to recover from surgery before experimental manipulation. For food intake studies, the animals were individually housed after surgery in order to collect food intake data. Otherwise, animals continued to be housed with their littermates. For rabies-tracing studies, mice were euthanized 1 week after rabies virus injection. Fluorescence reporters in all studies were used to confirm proper targeting of the brain region: if fluorescence was not observed within the region of interest, these cases were omitted from analyses. In the case of rabies tracing, the BST injection site was confirmed by visualizing inflammation and the needle track 1 week after injection, since the pseudotyped rabies virus requires tumor virus receptor A (TVA) expression for initial virus entry, and TVA expression was restricted to the VMN.

Optogenetic stimulation of VMN cells. Optogenetic fibers were placed 0.5 mm above the injection site for the VMN (AP: 1.2 mm, ML: 0.3 mm, and DV: 5.05 mm from bregma). Fibers were anchored above the skull with Metabond. Mice were allowed at least 4 weeks to recover from surgery before stimulation experiments. Laser stimulation (473 nm, MBL-F-473, Opto Engine) was performed at 5-ms pulses, 40 pulses per second for a total of 1 hour with an approximate irradiance 21 mW/mm^2. Parameters were chosen to match previous optogenetic stimulation studies in the VMN (2).

Determination of plasma epinephrine and norepinephrine concentrations. For the determination of plasma epinephrine and norepinephrine concentrations, 9 μL plasma was spiked with 1 μL of 12.5 mM ascorbic acid and 1 μL of a mixture containing 1 μM d6-epinephrine and d6-norepinephrine as internal standards to normalize for extraction efficiency and mass spectrometry ionization efficiency. Proteins were removed by the addition of 39 μL ice-cold acetonitrile, followed by centrifugation for 10 minutes at 12,100 ×g. A 20-μL aliquot of the supernatant was removed and benzoylated by sequential addition of 10 μL of 100 mM sodium carbonate, 10 μL benzoyl chloride (2% [v/v] in acetonitrile), and 10 μL sulfuric acid (1% [v/v] in 20% [v/v] acetonitrile in water) as previously described (35). Standard solu-

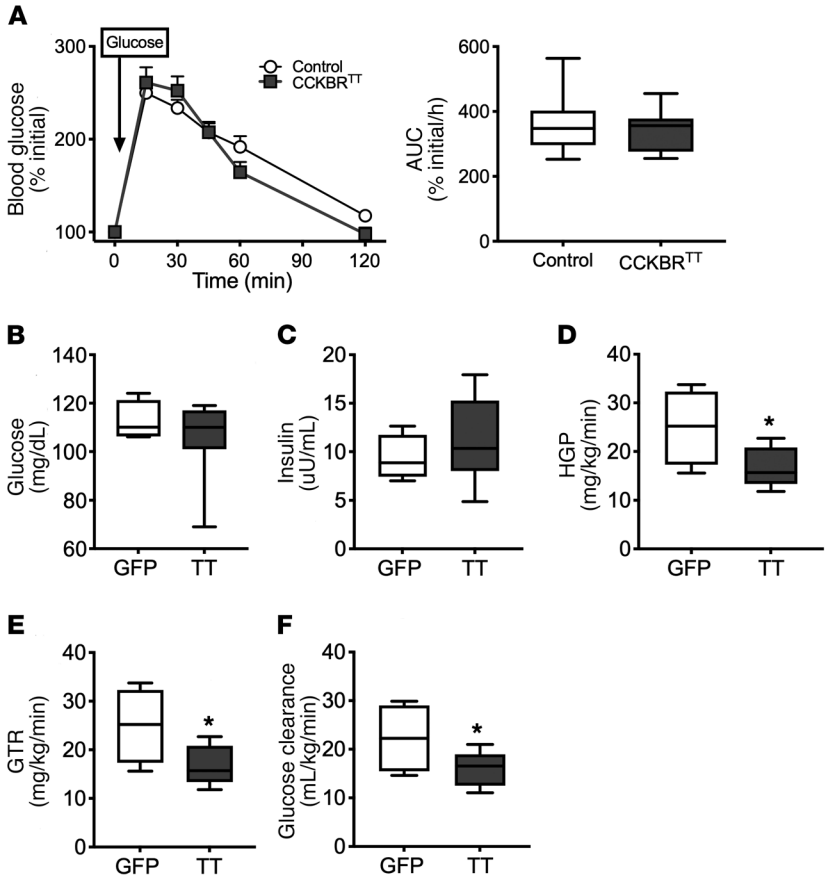

Figure 5. Silencing VMN^{CCKBR} neurons impairs HGP. AAV-DIO-TetTox-EGFP (CCKBR^{TT}) (n = 12) or AAV-GFP (control) (n = 30) was injected bilaterally into the VMN of *Cckbr*^{Cre} mice, and the effects on parameters of glucose homeostasis were assessed. (**A**) Blood glucose values and the calculated AUC for the GTT. (**B**–**F**) Animals were subjected to a basal clamp with infusion of 3H-glucose tracer and cold glucose to normalize glucose levels (**B**). Insulin was measured (**C**) and HGP (**D**), glucose turnover rate (GTR) (**E**), and glucose clearance (**F**) were calculated. Data are expressed as the percentage of initial blood glucose, because CCKBR^{TT} mice have lower baseline blood glucose levels than do controls; data expressed as raw blood glucose values are shown in Supplemental Figure 7. Data are expressed as the mean ± SEM (**A**, left) or as box-and-whisker plots showing the data spread from minimum to maximum, median, first quartile, and third quartile. *P < 0.05 versus control, by Student's t test.

tions of epinephrine and norepinephrine were prepared in artificial cerebrospinal fluid (ACSF), which is similar in salt composition to plasma without protein, to create a calibration range of 0.1–50 nM. Standards were spiked with the internal standard, diluted with acetonitrile, and derivatized as described above. Calibration curves were prepared on the basis of the peak area ratio of the standard to the internal standard by linear regression. All samples and standards were analyzed in triplicate using a Phenomenex Kinetex C18 Chromatography Column (100 × 2.1 mm, 1.7 μm, 100 Å) on a Vanquish Ultra-High-Performance Liquid Chromatograph (Thermo Fisher Scientific) interfaced to a TSQ Quantum Ultra Triple Quadrupole Mass Spectrometer (Thermo Fisher Scientific). Mobile phase A was 10 mM ammonium formate with 0.15% (v/v) formic acid in water. Mobile phase B was acetonitrile. The gradient used was as follows: initial, 5% B; 0.01 minutes, 19% B; 0.68 minutes, 26% B; 1.05 minutes, 75% B; 1.8 minutes, 100% B; 2.8 minutes, 100% B; 4 minutes, 5% B; and 5 minutes, 5% B at 600 μL/min. Benzoylated norepinephrine was eluted at 1.77 minutes, and benzoylated epinephrine was eluted at 1.81 minutes. The sample injection volume was 5 μL. The autosampler was kept at ambient temperature, and the column was held at 30°C in still air mode. Electrospray ionization was used in positive mode at 4 kV. The capillary temperature was 400°C, the vaporizer temperature was 350°C, the sheath gas was 10, and the auxiliary gas was 5. Ions were detected in tandem mass spectrometry (MS/MS) mode. For epinephrine and d6-epinephrine, the precursor ions were *m/z* 478 and 484, respectively, with the tube lens set to 93 and a collision energy of 26. For norepinephrine and d6-norepinephrine, the precursor ions were *m/z* 464 and 470, respectively, with a tube lens value of 81 and a collision energy of 19. The product ion was *m/z* 105 for all analytes. Automated peak integration was performed using XCalibur 3.0 MS software. All peaks were visually inspected to ensure proper integration.

Perfusion and IHC. Brains were collected and processed as previously described (21, 24). To reveal leptin-responsive neurons (p-STAT3), leptin (a gift from MedImmune) was administered (5 mg/kg, i.p.) 2 hours before perfusion. For all immunohistochemical and immunofluorescence analyses, mice were anesthetized with isoflurane before transcardial perfusion with PBS followed by 10% formalin. Brains were removed and placed into 10% formalin overnight, followed by 30% sucrose for at least 36 hours. Brains were cut into 30-μm sections on a freezing microtome in 4 series and stored in antifreeze solution (25% ethylene glycol, 25% glycerol). Sections were washed with PBS and then treated sequentially with 1% hydrogen peroxide/0.5% sodium hydroxide, 0.3% glycine, and 0.03% sodium dodecyl sulfate. Pretreatment was followed by 1 hour in blocking solution (PBS containing 0.1% triton, 3% normal donkey serum) and then overnight incubation in blocking solution containing chicken anti-GFP (1:1000, GFP-1020, Aves), rabbit anti-FOS (1:1000, sc-52, Santa Cruz Biotechnology), anti-dsRed (1:1000, 632496, Takara), and/or rabbit anti–p-STAT3 (1:500, 91455, Cell Signaling Technology). The next day, the sections were incubated with fluorescent secondary antibodies (1:200, Molecular Probes) or a biotinylated secondary antibody (1:200, Jackson ImmunoResearch) followed by ABC amplification (1:500, Vector Laboratories) and diaminobenzadine reaction (Thermo Fisher Scientific). The sections treated with a biotinylated

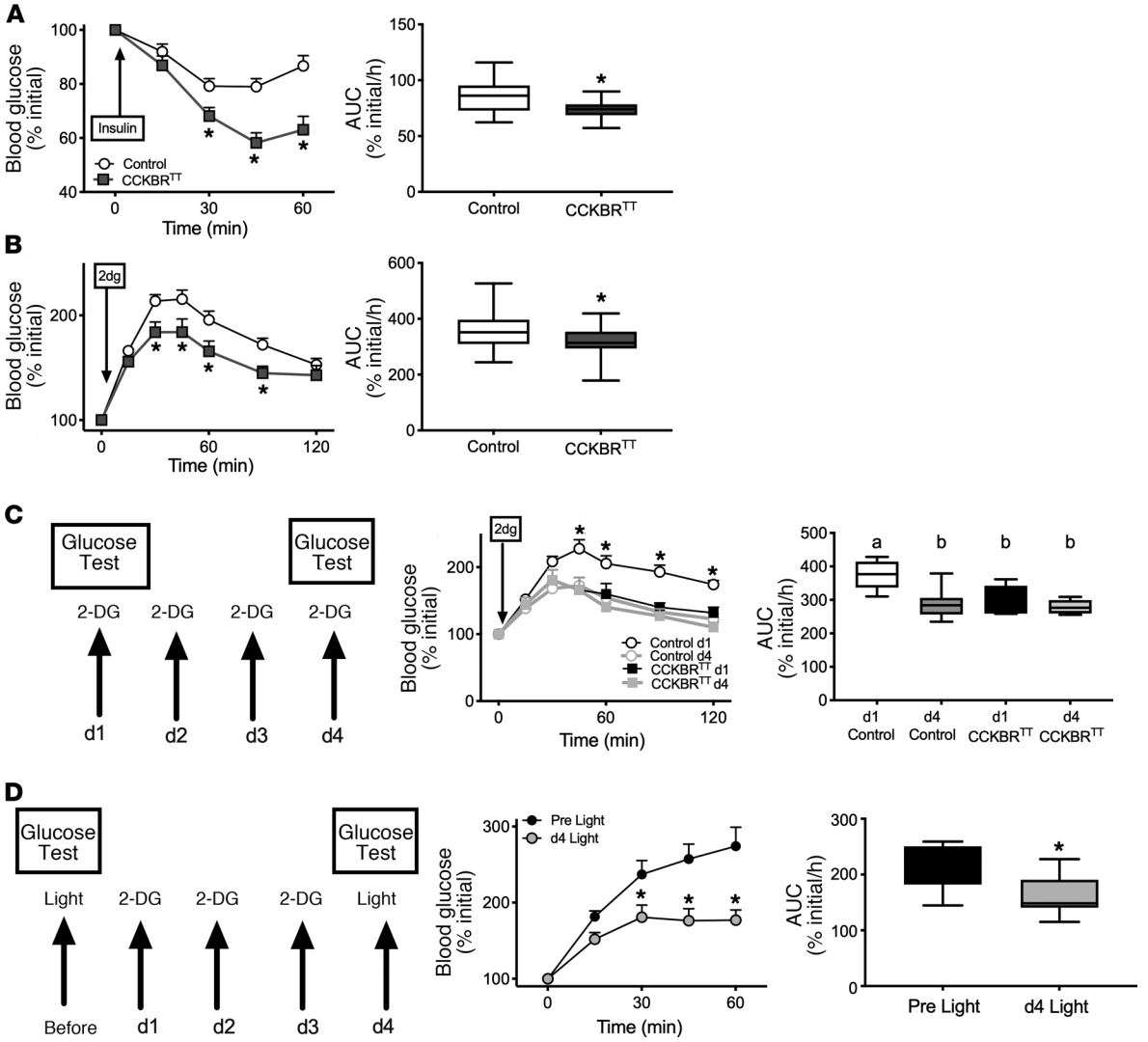

Figure 6. VMN^{CCKBR} neurons play a requisite role in the CRR. (**A** and **B**) Blood glucose values and the calculated AUC during insulin-induced hypoglycemia (0.6 U/kg, i.p.) (**A**) and in response to glucoprivation with 2-DG (250 mg/kg, i.p.) (**B**) for CCKBR^{TT} (n = 16) and control (n = 38) mice. Data in the left panels are expressed as the mean ± SEM, and AUC data are given as box-and-whisker plots that show the data spread from minimum to maximum, median, first quartile, and third quartile. *P < 0.05 versus control; time course data were analyzed by repeated-measures ANOVA with Fisher's LSD post hoc test, and AUC data were analyzed by Student's t test. (**C**) Response to repeated (daily for 4 days) glucoprivation with 2-DG (250 mg/kg, i.p.) in CCKBR^{TT} (n = 5) and control (n = 9) mice with glucose measurement during the subsequent 120 minutes on days 1 and 4. Data in the middle panel are expressed as the mean ± SEM, and AUC data are given as box-and-whisker plots showing the data spread from minimum to maximum, median, first quartile, and third quartile. *P < 0.05 versus the control; time course data were analyzed by repeated-measures ANOVA with Fisher's LSD post hoc test, and AUC data were analyzed by 1-way ANOVA with Fisher's LSD post hoc test. The different lowercase letters in the plots indicate significant differences (P < 0.05). (**D**) Response to repeated (daily for 3 days) glucoprivation with 2-DG (250 mg/kg, i.p.) in CCKBR^{ChR2} mice, with glucose levels measured during the subsequent 60 minutes on days 0 and 4. Note that mice from this experiment were the same as those described in Figure 1. Data in the middle panel are expressed as the mean ± SEM, and AUC data are given as box-and-whisker plots showing the data spread from minimum to maximum, median, first quartile, and third quartile; n = 9 for all. *P < 0.05 versus control; time course data were analyzed by repeated-measures ANOVA with Fisher's LSD post hoc test, and AUC data were analyzed by Student's t test.

secondary antibody were exposed to avidin/biotin complex solution followed by diaminobenzadine reaction. The sections were mounted onto slides coverslipped with Fluoromount-G (Southern Biotech). Most images were collected on an Olympus Bx53 microscope, and the number of immunoreactive cells was counted using Adobe Photoshop. For the images of CckbrEGFP-L10a sections throughout the brain (Supplemental Figure 1), sections were imaged on a Nikon A1 confocal microscope with a 10× dry (0.45 NA) objective and Nikon Elements Software, version 4.6. Fluorescence intensity was adjusted to near saturation of the Alexa Fluor 488–amplified, GFP-tagged CCKbR signal. Panoramic views through the coronal brain sections were captured by large format scans in XY arrays (typically 11 × 14 fields) with 5% overlap in XY, and a consistent signal in the z-focus plane was maintained by creating a z-focus map across each section. Adobe Photoshop and Illustrator were used to adjust brightness and contrast of the images and format the final composite monochrome figure.

Dual-label ISH and IHC. Dual-label ISH and IHC were performed essentially as previously described (36). Briefly, free-floating

sections from adult males were treated with 0.1% sodium borohydride for 15 minutes and 0.25% acetic anhydride in DEPC-treated 0.1 M triethanolamine (TEA), pH 8.0, for 10 minutes. Sections were incubated overnight at 50°C in the hybridization solution (50% formamide, 10 mM Tris-HCl, pH 8.0, 5 mg tRNA, 10 mM DTT, 10% dextran sulfate, 0.3 M NaCl, 1 mM EDTA, and 1× Denhardt's Solution [Thermo Fisher Scientific]) containing the ^{35}S-labeled *Cckbr* riboprobe. Subsequently, sections were treated with RNAse A for 30 minutes and submitted to stringency washes in sodium chloride-sodium citrate (SSC) buffer. Sections were blocked in 3% BSA (in PBS-Triton) and then incubated with a chicken anti-GFP (as above) antibody overnight at 4°C. Sections were incubated for 1.5 hours in donkey anti–chicken IgG–linked AF594 (Alexa Fluor, Life Technologies, Thermo Fisher Scientific) and then mounted onto Superfrost Plus slides (Thermo Fisher Scientific, dehydrated in increasing concentrations of ethanol, dipped in NTB-2 autoradiographic emulsion (Kodak), and dried and stored in light-protected boxes at 4°C for 3 weeks. Slides were developed with D-19 developer (Kodak), dehydrated in graded ethanol, cleared in xylenes, and coverslipped with DPX mounting medium (Sigma-Aldrich).

Pancreatic β cell mass determination. Pancreata were dissected out and fixed in 3.7% formalin overnight before paraffin embedment. For each animal, 5 random sections per pancreas, at least 250-μm apart, were deparaffinized, microwaved for 4 minutes in a sodium citrate/citric acid solution for antigen retrieval, permeabilized for 20 minutes in TBS 0.1% Triton-100, incubated for 230 minutes in a blocking solution (11096176001, Roche), incubated overnight with anti-insulin primary antibody (1:800, A0564, Agilent Technologies) in blocking solution, washed in TBS-Tween, and then incubated for 2 hours at room temperature with a fluorescent FITC-conjugated anti–guinea pig secondary antibody (1:400, 706-095-148, Immunotech, Jackson ImmunoResearch) in blocking solution before final washes and mounting with an antifading mounting solution. Images were acquired on a Nikon AZ-100 microscope with a motorized stage using the NIS-Elements BR, version 4 (Nikon Instruments). NIS Elements automatically assembled the mosaics (15% overlap) required to capture the entire pancreatic cross sections. The β cell area was determined by intensity thresholding using the Fiji 2.0.0-rc-69 morphometry measurement tools (37, 38), as previously described (39). β Cell mass was calculated as the product of the percentage of the insulin-immunoreactive area by the total weight of the organ.

Phenotypic studies. BW and food intake were monitored weekly in animals after surgery. Glycemic measurements, including a GTT (2 g/kg BW, i.p.), IIH (0.6 unit/kg BW, i.p. Humulin, Eli Lilly), and 2-DG (Sigma-Aldrich) challenge (250 mg/kg BW, i.p.) were determined in 12- to 18-week-old animals by analyzing tail vein blood and using a OneTouch Ultra 2 glucometer (Johnson & Johnson). For all glycemic tests, mice were fasted for 4 to 6 hours before testing. To measure leptin-induced p-STAT3 levels, animals were fasted for 24 hours before leptin administration. Body fat and lean mass were analyzed in a cohort of mice using a MiniSpec LF9011 (Bruker Optics). The same animals were also subjected to the Comprehensive Laboratory Animal Monitoring System (CLAMS) (Columbus Instruments) 12 weeks after injection in order to measure oxygen consumption (VO_2) and activity. Body composition and CLAMs data were collected with assistance from the University of Michigan's Mouse Metabolic Phenotyping Center. Glucagon, insulin, and leptin were assayed with a commercial ELISA (glucagon, Mercodia; leptin and insulin, Crystal Chem). Corticosterone levels were determined by radioimmunoassay (MP Biomedicals) with assistance from the Chemistry Core supported by the Michigan Diabetes Research Center at the University of Michigan.

STZ treatment. STZ (160 mg/kg, i.p., Sigma-Aldrich) was administered weekly. STZ was administered immediately following the addition of freshly made pH 4.5, 0.1 M sodium citrate buffer. Mice were provided 10% sucrose solution to drink to prevent severe hypoglycemia induced by insulin surges.

Basal glucose clamps. Under anesthesia, mice were catheterized with silicon tubing. After surgery, mice were housed individually, and their BW was monitored daily. Mice that lost more than 10% of their presurgery BW were removed from the study. On the day of data collection, mice were fasted for 5 to 6 hours starting 1.5 hours after lights-on. The basal clamp consisted of a 90-minute equilibration period with infusion of 50% [3-3H]glucose at variable rates to maintain euglycemia. Plasma radioactivity of [3-^{3}H]glucose and plasma insulin levels were analyzed as previously described (40).

HAAF induction protocol. Mice were treated on consecutive days with 2-DG (250 mg/kg, i.p., Sigma-Aldrich). On each day, mice were fasted before 2-DG administration for at least 4 hours starting at lights-on. On days 1 and 4, blood glucose levels were determined in a manner similar to other glycemic measurements using the OneTouch Ultra 2 glucometer (Johnson & Johnson). Food was returned to each mouse at least 2 hours after 2-DG treatment.

Statistics. Statistical tests were not used to predetermine sample sizes, but our sample sizes were similar to those of previously published studies in which similar approaches were used (21, 34, 41–43). Time course blood glucose, BW, and food intake data were analyzed using a 2-way, repeated-measures ANOVA with Fisher's least significant difference (LSD) post hoc test. Data in Figure 1D, Figure 3, A–D, and Figure 4 were analyzed with a 2-way ANOVA. Hormone data in Figure 1, E–I, clamp data in Figure 5, and AUC data were analyzed by Student's *t* test. Data in Figure 2, D–F, were analyzed by 1-way ANOVA. No data were removed unless the injection was a miss or the animal was sick or injured at the time of the experiment (loss of >10% BW). Significance was set at a P value of 0.05 or less. All data were analyzed using GraphPad Prism software (GraphPad Software).

Study approval. The procedures in this study were approved by the IACUC of the University of Michigan in accordance with Association for Assessment and Accreditation of Laboratory Animal Care (AAALAC) policies.

Author contributions

JNF, PBG, JDO, PVS, NB, MS, AV, AR, AHA, CCM, AA, JS, and NK performed research and analyzed data. JNF, PBG, CL, DAS, RTK, DPO, and MGM designed experiments and wrote and edited the manuscript. All authors reviewed and edited the manuscript. MGM is the guarantor of the manuscript.

Acknowledgments

We thank B. Roth and K. Deisseroth for the AAV plasmid constructs. We thank Randy Seeley, Michael Schwartz, Kevin Grove, Mads Tang-Christensen, Christine Bjørn Jensen, and members of the Myers and Olson laboratories for helpful discussions. Research

support was provided by the Michigan Diabetes Research Center (NIH grant P30 DK020572, including the Molecular Genetics, Microscopy, and Animal Studies Cores); the American Diabetes Association (17-INI-15, to JNF); the Marilyn H. Vincent Foundation (to MGM); and Novo Nordisk (to MGM). This work was also supported in part by NIH grants DK082480 (to DAS), DK104999 (to DPO), EB003320 (to RTK), and DK122660 (to AHA), and R25 DK088752 (to AA).

Address correspondence to: Martin G Myers, Jr., 1000 Wall St; 6317 Brehm Tower, Ann Arbor, Michigan 48105, USA. Phone: 734.647.9515; Email: mgmyers@umich.edu.

1. Bernard C. Chiens rendus diabetiques. *C R Soc Biol (Paris)*. 1849;1(14):60–63.
2. Meek TH, et al. Functional identification of a neurocircuit regulating blood glucose. *Proc Natl Acad Sci USA*. 2016;113(14):E2073–E2082.
3. Stanley SA, et al. Bidirectional electromagnetic control of the hypothalamus regulates feeding and metabolism. *Nature*. 2016;531(7596):647–650.
4. Schwartz MW, et al. Cooperation between brain and islet in glucose homeostasis and diabetes. *Nature*. 2013;503(7474):59–66.
5. McCrimmon RJ, Sherwin RS. Hypoglycemia in type 1 diabetes. *Diabetes*. 2010;59(10):2333–2339.
6. Dagogo-Jack SE, Craft S, Cryer PE. Hypoglycemia-associated autonomic failure in insulin-dependent diabetes mellitus. Recent antecedent hypoglycemia reduces autonomic responses to, symptoms of, and defense against subsequent hypoglycemia. *J Clin Invest*. 1993;91(3):819–828.
7. Tong Q, et al. Synaptic glutamate release by ventromedial hypothalamic neurons is part of the neurocircuitry that prevents hypoglycemia. *Cell Metab*. 2007;5(5):383–393.
8. Watts AG, Donovan CM. Sweet talk in the brain: glucosensing, neural networks, and hypoglycemic counterregulation. *Front Neuroendocrinol*. 2010;31(1):32–43.
9. Ritter S, Li AJ, Wang Q, Dinh TT. Minireview: the value of looking backward: the essential role of the hindbrain in counterregulatory responses to glucose deficit. *Endocrinology*. 2011;152(11):4019–4032.
10. Levin BE, Routh VH, Kang L, Sanders NM, Dunn-Meynell AA. Neuronal glucosensing: what do we know after 50 years? *Diabetes*. 2004;53(10):2521–2528.
11. Viskaitis P, et al. Modulation of SF1 neuron activity coordinately regulates both feeding behavior and associated emotional states. *Cell Rep*. 2017;21(12):3559–3572.
12. Hawke Z, Ivanov TR, Bechtold DA, Dhillon H, Lowell BB, Luckman SM. PACAP neurons in the hypothalamic ventromedial nucleus are targets of central leptin signaling. *J Neurosci*. 2009;29(47):14828–14835.
13. Toda C, Kim JD, Impellizzeri D, Cuzzocrea S, Liu ZW, Diano S. UCP2 regulates mitochondrial fission and ventromedial nucleus control of glucose responsiveness. *Cell*. 2016;164(5):872–883.
14. Kim JD, Toda C, Ramírez CM, Fernández-Hernando C, Diano S. Hypothalamic ventromedial Lin28a enhances glucose metabolism in diet-induced obesity. *Diabetes*. 2017;66(8):2102–2111.
15. Fujikawa T, et al. SF-1 expression in the hypothalamus is required for beneficial metabolic effects of exercise. *Elife*. 2016;5:e18206.
16. Toda C, et al. Extracellular signal-regulated kinase in the ventromedial hypothalamus mediates leptin-induced glucose uptake in red-type skeletal muscle. *Diabetes*. 2013;62(7):2295–2307.
17. Dhillon H, et al. Leptin directly activates SF1 neurons in the VMH, and this action by leptin is required for normal body-weight homeostasis. *Neuron*. 2006;49(2):191–203.
18. Minokoshi Y, Haque MS, Shimazu T. Microinjection of leptin into the ventromedial hypothalamus increases glucose uptake in peripheral tissues in rats. *Diabetes*. 1999;48(2):287–291.
19. Gavini CK, Jones WC, Novak CM. Ventromedial hypothalamic melanocortin receptor activation: regulation of activity energy expenditure and skeletal muscle thermogenesis. *J Physiol (Lond)*. 2016;594(18):5285–5301.
20. Garfield AS, et al. A parabrachial-hypothalamic cholecystokinin neurocircuit controls counterregulatory responses to hypoglycemia. *Cell Metab*. 2014;20(6):1030–1037.
21. Flak JN, et al. Leptin-inhibited PBN neurons enhance responses to hypoglycemia in negative energy balance. *Nat Neurosci*. 2014;17(12):1744–1750.
22. Moran TH, Ladenheim EE. Adiposity signaling and meal size control. *Physiol Behav*. 2011;103(1):21–24.
23. Wall NR, Wickersham IR, Cetin A, De La Parra M, Callaway EM. Monosynaptic circuit tracing in vivo through Cre-dependent targeting and complementation of modified rabies virus. *Proc Natl Acad Sci USA*. 2010;107(50):21848–21853.
24. Flak JN, et al. A leptin-regulated circuit controls glucose mobilization during noxious stimuli. *J Clin Invest*. 2017;127(8):3103–3113.
25. Adamantidis AR, Zhang F, Aravanis AM, Deisseroth K, de Lecea L. Neural substrates of awakening probed with optogenetic control of hypocretin neurons. *Nature*. 2007;450(7168):420–424.
26. Han S, Soleiman MT, Soden ME, Zweifel LS, Palmiter RD. Elucidating an affective pain circuit that creates a threat memory. *Cell*. 2015;162(2):363–374.
27. Morton GJ, Meek TH, Matsen ME, Schwartz MW. Evidence against hypothalamic-pituitary-adrenal axis suppression in the antidiabetic action of leptin. *J Clin Invest*. 2015;125(12):4587–4591.
28. Berglund ED, et al. Direct leptin action on POMC neurons regulates glucose homeostasis and hepatic insulin sensitivity in mice. *J Clin Invest*. 2012;122(3):1000–1009.
29. Rossetti L, et al. Short term effects of leptin on hepatic gluconeogenesis and in vivo insulin action. *J Biol Chem*. 1997;272(44):27758–27763.
30. Scheurink A, Ritter S. Sympathoadrenal responses to glucoprivation and lipoprivation in rats. *Physiol Behav*. 1993;53(5):995–1000.
31. Zhu W, et al. Glucose prevents the fall in ventromedial hypothalamic GABA that is required for full activation of glucose counterregulatory responses during hypoglycemia. *Am J Physiol Endocrinol Metab*. 2010;298(5):E971–E977.
32. Coutinho EA, et al. Activation of SF1 neurons in the ventromedial hypothalamus by DREADD technology increases insulin sensitivity in peripheral tissues. *Diabetes*. 2017;66(9):2372–2386.
33. Chan O, et al. Increased GABAergic output in the ventromedial hypothalamus contributes to impaired hypoglycemic counterregulation in diabetic rats. *Diabetes*. 2011;60(5):1582–1589.
34. Allison MB, Patterson CM, Krashes MJ, Lowell BB, Myers MG, Olson DP. TRAP-seq defines markers for novel populations of hypothalamic and brainstem LepRb neurons. *Mol Metab*. 2015;4(4):299–309.
35. Mabrouk OS, Semaan DZ, Mikelman S, Gnegy ME, Kennedy RT. Amphetamine stimulates movement through thalamocortical glutamate release. *J Neurochem*. 2014;128(1):152–161.
36. Williams KW, et al. The acute effects of leptin require PI3K signaling in the hypothalamic ventral premammillary nucleus. *J Neurosci*. 2011;31(37):13147–13156.
37. Schindelin J, et al. Fiji: an open-source platform for biological-image analysis. *Nat Methods*. 2012;9(7):676–682.
38. Schneider CA, Rasband WS, Eliceiri KW. NIH Image to ImageJ: 25 years of image analysis. *Nat Methods*. 2012;9(7):671–675.
39. Cras-Méneur C, Li L, Kopan R, Permutt MA. Presenilins, Notch dose control the fate of pancreatic endocrine progenitors during a narrow developmental window. *Genes Dev*. 2009;23(17):2088–2101.
40. Chen Z, et al. Insulin resistance and metabolic derangements in obese mice are ameliorated by a novel peroxisome proliferator-activated receptor γ-sparing thiazolidinedione. *J Biol Chem*. 2012;287(28):23537–23548.
41. Leinninger GM, et al. Leptin action via neurotensin neurons controls orexin, the mesolimbic dopamine system and energy balance. *Cell Metab*. 2011;14(3):313–323.
42. Leshan RL, Greenwald-Yarnell M, Patterson CM, Gonzalez IE, Myers MG. Leptin action through hypothalamic nitric oxide synthase-1-expressing neurons controls energy balance. *Nat Med*. 2012;18(5):820–823.
43. Patterson CM, et al. Ventral tegmental area neurotensin signaling links the lateral hypothalamus to locomotor activity and striatal dopamine efflux in male mice. *Endocrinology*. 2015;156(5):1692–1700.